Hierarchical Control for Multiple DC Microgrids Clusters

Shafiee, Qobad; Dragicevic, Tomislav; Vasquez, Juan Carlos; Guerrero, Josep M.

Published in:
I E E E Transactions on Energy Conversion

DOI (link to publication from Publisher):
10.1109/TEC.2014.2362191

Publication date:
2014

Document Version
Early version, also known as pre-print

This document is a preprint of the final paper:
Q. shafiee, T. Dragicevic, J. C. Vasquez, and J. M. Guerrero, "Hierarchical Control for Multiple DC-Microgrids Clusters," IEEE Transaction on Energy Conversion, 2014.

Hierarchical Control for Multiple DC-Microgrids Clusters

Qobad Shafiee, *Student Member, IEEE*, Tomislav Dragicevic, *Student Member, IEEE*, Juan C. Vasquez, *Member, IEEE*, and Josep M. Guerrero, *Senior Member, IEEE*

***Abstract*—This paper presents a distributed hierarchical control framework to ensure reliable operation of dc Microgrid (MG) clusters. In this hierarchy, primary control is used to regulate the common bus voltage inside each MG locally. An adaptive droop method is proposed for this level which determines droop coefficients according to the state-of-charge (SOC) of batteries automatically. A small signal model is developed to investigate effects of the system parameters, constant power loads as well as line impedance between the MGs on stability of these systems. In the secondary level, a distributed consensus-based voltage regulator is introduced to eliminate the average voltage deviation over the MGs. This distributed averaging method allows the power flow control between the MGs to be achieved at the same time, as it can be accomplished only at the cost of having voltage deviation inside the system. Another distributed policy is employed then to regulate the power flow among the MGs according to their local SOCs. The proposed distributed controllers on each MG communicate with only the neighbor MGs through a communication infrastructure. Finally, the small signal model is expanded for dc MG clusters with all the proposed control loops. The effectiveness of proposed hierarchical scheme is verified through detailed hardware-in-the-loop (HIL) simulations.**

***Index Terms*—DC microgrid, hierarchical control, adaptive droop, stability analysis, distributed control, voltage control, power flow control.**

I. Introduction

DC Microgrids have gained research interest recently to facilitate integrating of modern electronic loads and alternative energy sources with dc output type such as photovoltaic (PV) systems, fuel cells, and energy storage systems (e.g., secondary battery and super capacitor) [1]–[7]. Normally, dc MGs are proposed for power supply of applications with sensitive and/or dc loads like consumer electronics, electric vehicles, naval ships, space crafts, submarines, telecom systems and rural areas which benefits from increased power quality, and higher reliability and efficiency.

The advantages of dc MGs are summarized as 1) the conversion losses from sources to loads are reduced, thus enhancing the system efficiency; 2) there is no need for control of frequency and phase, reactive power, and power quality, which are all big challenges in ac MGs. Furthermore, synchronization requirements for connection of distributed generators (DGs) and energy storage systems (ESSs) to the bus and the main grid are not an issue in dc MGs; 3) in the grid connection mode, any blackout or voltage sag that may happen from the grid side does not affect the units inside the MG. Nevertheless, protection is still a big challenge in this new concept for dc systems and it is normally needed to construct new dc distribution lines while implementing dc MGs [1].

Although there is a significant increase of dc MG research works nowadays, we can still find lack of studies about modeling, stability analysis, and control of these kinds of systems. A hierarchical multilevel control strategy has been introduced for dc MGs with three levels: primary, secondary and tertiary control [7]. The primary control, which is strictly local, deals with the inner control loops and droop control of the dc sources. In this level, droop control which is a resistive virtual loop, provides the voltage reference to the inner control loops. However, droop control is not always the best control strategy for renewable energy sources (RESs) and ESSs where it is preferred to absorb/inject specified power from/to them. The secondary control sets the reference of primary control such that deviations produced by the droop control are eliminated to maintain the dc MG voltage within the acceptable values. The tertiary control is responsible for managing the current flow from/to an external dc source, which can be a dc distribution system, another dc or ac MG, or dc/ac converter connected to the main grid.

In the primary level, droop coefficient is normally defined according to the ratings of power converters. However, sometimes is better to share power between the units in different ways. In this regard, several adaptive droop methods have been presented recently [8]–[12]. An adaptive droop scheme is proposed for multi-terminal dc grids in [8] to share the load according to the available headroom of converters. The authors in [9] propose a control strategy based on fuzzy logic that assures good storage energy balance and low voltage deviation for a low voltage DC MG, by modifying the droop coefficients in accordance with the SOC of each energy storage unit. In [10], a SOC dependent function is introduced only for discharging mode of ESSs inside a MG, while two separate functions have been presented for both charging and discharging mode of battery according to its capacity and the SOC in [11]. Similarly, a double-quadrant SOC-based droop control method is proposed in [12] which guarantees SOC balancing and output power equalization in both charging and discharging modes.

The secondary and tertiary controls are typically centralized [7], and require communication network with full connectivity. Although it is easy implementing, scalability of the centralized control strategy is not straightforward and it has an inherent

Q. Shafiee, T. Dragicevic, J. C. Vasquez, and J. M. Guerrero are with the Institute of Energy Technology, Aalborg University, Aalborg East DK-9220, Denmark, (e-mail: qsh@et.aau.dk, tdr@et.aau.dk, juq@et.aau.dk, joz@et.aau.dk)

drawback of the single point of failure. Distributed control has attracted a lot of interests as an alternative recently, as it provides easier scalability, simpler communication network, and improved reliability [13], [14].

Distributed control approaches are well known as scalable and robust approaches where a series of local exchanges among neighboring units ultimately yield the same global information at every unit. Several distributed control methods have been introduced in the literature from which consensus-based [15] and gossip [16] algorithms have recently received significant attention mostly because of their simplicity and robustness for distributed information processing over networks. The usage of these distributed algorithms for dc systems and dc MG application has been considered recently [13], [17]–[20]. A distributed control method is proposed in [17] for current sharing in dc MGs. This distributed approach is based on averaging the total current supplied by the sources. In [18], similar distributed method is proposed based on average voltage and average current of the sources to enhance the load current sharing accuracy and restore the local dc output voltage. Although in these works the controllers are embedded locally, all sources must communicate with all other sources in order to calculate the average of information, and hence the method still requires complicated communication. In addition, the gains of the controllers must be finely tuned in order to provide accurate performance. In [19], a consensus-based distributed load sharing method is introduced for parallel dc-dc converters, to avoid using a master converter or a central controller. A fully distributed secondary/primary controller based on consensus protocols is introduced in [13] for voltage regulation and proportional current sharing of dc MGs considering line impedances. The control paradigms proposed in above mentioned distributed works use sparse communication network for data exchange between the converters. Moreover, application of distributed consensus-based algorithms for tertiary control of dc MGs has been presented recently [20], where a distributed optimization method is introduced to improve the system efficiency.

Another alternative to increase the reliability is to establish dc MG clusters by connecting neighbor MGs. This way, each MG will be able to absorb power from its neighbors in the case of emergency situation. Nevertheless, interconnecting dc MGs sometimes tends to destabilize the system. Several works have been proposed to address stability of power electronic converters and MG applications [21]–[23]. However, no research works has been done to analysis and improve the stability of MGs while they are connected. Moreover, overall control of these systems, voltage regulation, and control of power flow between the MGs is still open to research.

This paper proposes a distributed hierarchical control scheme for dc MG clusters. In the primary level which is decentralized, dc bus voltage is regulated and current sharing between sources in the MG can be achieved. To improve efficiency of parallel batteries inside MGs, an adaptive droop method is presented which defines droop coefficient automatically according to SOC of batteries. Moreover, a small signal stability model is developed in order to study impact of different parameters of the system. As power flow control is achieved only at the expense of voltage deviations inside the system, a consensus-based distributed voltage regulator is proposed in the secondary level. The voltage regulator acts as a centralized controller for each MG; however, it becomes distributed over the multiple MGs when they are connected and power flow control is required. A distributed power flow controller is introduced then which uses the average SOC of local MGs in order to regulate the tie-line current reference automatically. Finally, the effectiveness of the proposed scheme is verified by HIL simulation study.

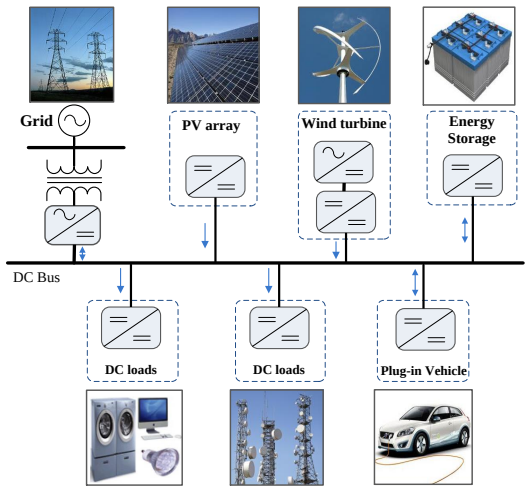

Fig. 1. Typical configuration of a low-voltage dc Microgrid.

The remainder of the paper is organized as follows: Section II presents configuration of a dc MG. After a general overview of primary control, the proposed adaptive droop control and small signal modeling are presented in Section III. Section IV introduces the distributed voltage regulator and power flow controller. Section V studies performance of the proposed controller for interconnected MG clusters. Section VI concludes the paper.

II. DC MICROGRID CONFIGURATION

Normally a dc MG consists of distributed energy resources (DERs) and ESSs which are supplying electronic and other kinds of loads through a common dc bus. Fig. 1 shows a general configuration of low-voltage dc (LVDC) Microgrids. DERs used in an LVDC microgrid can be of various types, such as PV arrays, fuel cells (FC), wind-turbine (WT) generators, and microturbines. PV and FC are more appropriate to be used in dc MGs since they produce dc voltage. However, WT and microturbine which generate voltage with varying frequency, require conversion to be connected to the dc bus and used in dc MGs.

On the other hand, due to transient response of sources, and the fact that they cannot be always available (in the case of RESs), ESSs are mandatory to be connected to the dc MG if it is operated in islanded mode [11]. Furthermore, they can be used for ancillary services like voltage regulation, power quality improvement and emergency power supply. Normally secondary batteries, super capacitors, and flywheels are used as an ESS. Batteries and capacitors can be directly connected to the dc bus, but flywheels are connected through a machine

and a converter [6]. Nevertheless, it is desired to connect the ESSs to the dc bus through converters for full controllability.

The common bus is linked to the sources through the power electronic interfaces. Depending on the source type and voltage, there could be one or two stages of power conversion as shown in Fig. 1. To connect different sources and loads to the dc MG, different dc-dc converters with different characteristics must be used. The structure of these converters is simpler than ac-dc one, which results in higher efficiency and lower cost. Comparing to the ac MG, dc one requires fewer power converters, and it is more naturally interfaced to the sources [24].

III. Primary Control

Primary control is employed locally for every source inside the MG in order to control the current injection into the common bus automatically. This level of control is generally made of inner control loops and droop control, as shown in Fig. 2.

A. Inner Control Loops

Inner control loops are deployed as a first step of control based on direct measurements in order to regulate the voltage and current while maintaining the system stable. These loops comprise two control loops in general; the outer one is responsible for producing current reference and the inner one regulates the output current to follow that reference. Depending on the type of source inside the MG and the condition it has, the outer loop could have different forms such as maximum power point tracking (MPPT) mode for RESs, charging control strategy for ESSs, and voltage control loop.

MPPT techniques are usually essential part of RES control systems from which they automatically find the voltage or current to obtain the maximum power output under given environmental conditions [25]. On the other hand, charging control strategies are applied to the connected batteries in order to recover their SOC [26]. RESs operating in MPPT mode and batteries in regulated charging mode act as a current source converter (CSC) as they extract a constant power in any condition. The former behaves as a constant power source (CPS) while the latter acts as a constant power load (CPL) [11]. Therefore, both control strategies are modeled as an adjustable current reference to produce set-point for the current inner loop as shown in Fig. 2. Normally, the inner control loops employ proportional-integral (PI) regulators as they are easy to be implemented.

As control of dc bus voltage is a priority in the MGs, some of the units must operate as voltage source converter (VSC). Although RESs can also operate as a VSC to participate in the voltage support, batteries are the best choice for use as a VSC because of their bidirectional capability. An outer loop called droop control is normally employed to be added to the inner control loops for parallel connection of these VSCs inside the MG.

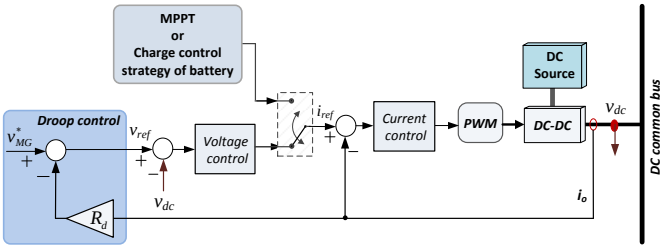

Fig. 2. Primary control of DC MGs.

B. Conventional Droop Control

In dc MGs, a virtual output resistance loop representing droop control is implemented on the top of inner loops in order to connect a number of sources in parallel thus sharing load current between the units. In this decentralized control strategy, a proportional part of the output current is subtracted from the output voltage reference to generate a reference for the inner voltage loop. This virtual loop will reduce the circulating current produced by physical differences between converters and lines. Moreover, it improves the dynamic performance of the output voltage [7]. This control loop creates appropriate reference for the voltage inner loop as follows

$$v_{ref} = v^*_{MG} - R_d \cdot i_o \tag{1}$$

with v^*_{MG} being MG voltage reference, i_o is the output current and R_d is the virtual resistance. The value of virtual resistance determines how power is shared among sources in the MG. The main drawback of droop method is poor voltage regulation. Once the power/current sharing is improved among the MG units, the voltage drop increases. The larger droop gain is, the more voltage deviation and the more accurate is load sharing between the sources. In addition, instability of MG is more likely with the small value of R_d. Therefore, the droop method has an inherent trade-off between stability, voltage regulation and load sharing.

Although in conventional method a fixed droop coefficient can be defined according to the ratings of individual converter, sometimes is needed to share currents in different ways.

C. Adaptive Droop Control

In islanded MG systems, batteries mostly operate in droop control mode as they are able to handle the power difference between RES production and load consumption automatically. For this type of EESs, it is preferred participating in power sharing according to their SOCs as SOC equalization can be achieved among connected batteries [10]. This way, life-cycle of batteries may improve as the batteries with small depth of charge are expected to have better life-cycle [26].

In order to equalize the SOCs in a general MG system, a battery with higher SOC should have dominant contribution in power sharing thus discharging at the most quick rate whereas the ones with lower SOC should be discharged with slowest rate participating lesser in the load sharing. The strategy is in contrary for charging mode. To do this, a new function is proposed here from which the droop coefficient of each battery (R^i_d), is adapted according to its current SOC. Moreover, battery capacity is also taken into account as it is inversely

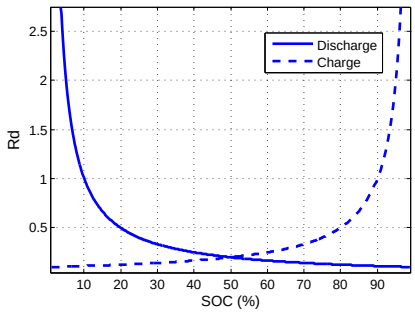

Fig. 3. Proposed charge and discharge functions for adapting droop control.

proportional to the changing rate of SOC. Therefore, droop coefficients are computed for charge and discharge conditions separately as follows:

$$\begin{cases} R^i_{d,\,charge} = \frac{C_{bi}}{C_{b\max}} \cdot \alpha \cdot (\frac{100}{100-SOC_i})^k \\ \\ R^i_{d,\,discharge} = \frac{C_{bi}}{C_{b\max}} \cdot \alpha \cdot (\frac{100}{SOC_i})^k \end{cases} \tag{2}$$

where C_{bi} is the nominal capacity of battery i, $C_{b\max}$ is the capacity of the battery with highest nominal capacity in the system, k and α are positive constants which determine the SOC-balancing speed and minimum value of droop coefficient, respectively. It should be noted that as the highest nominal capacity is only a constant parameter which is the same in (2) for all the batteries, even if the biggest battery fails, the others can still work properly.

Relationship between droop coefficient and SOC, presented in (2), is indicated in Fig. 3 for $k = 1$ and $\alpha = 0.1$. As Fig. 3 indicates, the higher R_d is given to the battery with higher SOC when batteries are charging and it is allocated to one with lower SOC when discharging. Moreover, faster charge/discharge rate can be observed at the end (beginning) of charging (discharging) mode. It is worth mentioning that some constraints must be taken into account while defining parameters of the functions (k and α) with respect to the mentioned droop control limitations.

There exist several advanced methods to estimate SOC [27]. Here we use ampere counting method which describes as follows

$$SOC_i(t) = SOC_i(0) - \frac{\eta_i}{C_{bi}} \int_0^t I_i(\tau)\, d\tau \tag{3}$$

where I_i is battery current, η_i is charging/discharging efficiency, and $SOC_i(0)$ is initial SOC. Control diagram of the proposed adaptive droop scheme implemented on primary control of an individual connected battery (battery i) inside a MG is shown in Fig. 4.

Simulation results of implementing the proposed adaptive droop method on two parallel batteries inside a MG are presented in the following figures. The MG includes two batteries and two RESs supporting some loads. The capacity of batteries is considered to be 0.05 Ah to speed up the simulations. The waveforms of SOC and input/output power of each converter are indicated in Fig. 5 and Fig. 6, for the proposed charging and discharging function of adaptive droop respectively, when $k = 2$ and $\alpha = 0.01$. As shown, in both

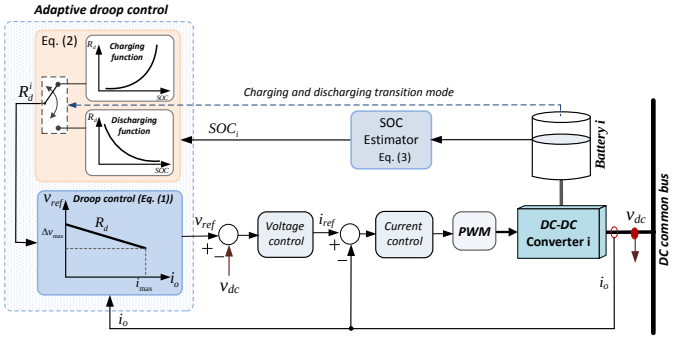

Fig. 4. Control diagram of the proposed adaptive droop control scheme.

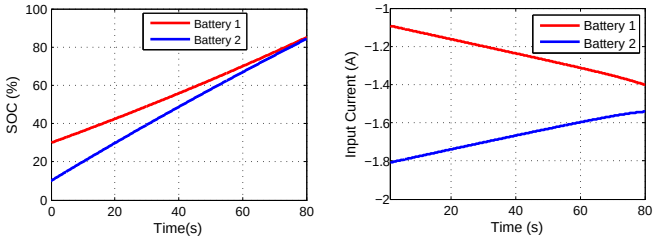

(a) (b)

Fig. 5. Performance of the proposed adaptive droop control in charging mode. (a) SOC1 and SOC2. (b) Input current of batteries.

modes, the battery with higher SOC absorbs/delivers more power than the one with lower. As a result, SOCs trends to be equalized, while sharing the total power. Similar waveforms are presented in Fig. 7(a) for various initial differences in the SOCs; SOC of battery 1 is set to 10 while SOC of battery 2 varies from 30 to 70. These waveforms are the same for both charging and discharging functions. Convergence speed of the adaptive method is investigated for different values of exponent k and fixed value of $\alpha = 0.01$ in Fig. 7(b).

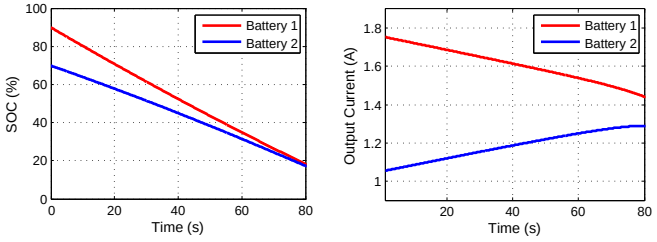

(a) (b)

Fig. 6. Performance of the proposed adaptive droop control in discharging mode. (a) SOC1 and SOC2. (b) Output current of batteries.

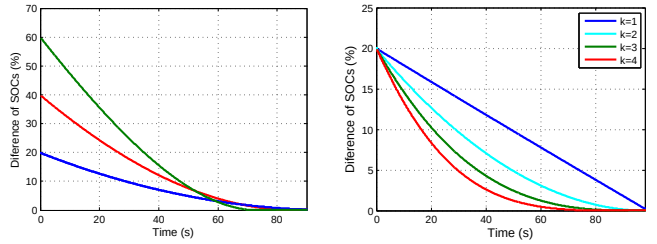

(a) (b)

Fig. 7. Evaluation of the proposed adaptive droop for: (a) Different initial SOCs. (b) Different values of exponent k.

It is obvious that, the larger exponent k, the faster SOC equalization and hence the accurate power sharing. The results show that the proposed adaptive droop function is faster and more flexible than one presented in [11].

It is worth mentioning that in practical systems in which the energy sources are only renewables, required battery capacity needs to be high enough to maintain the power balance at all times [28]. In this paper, droop coefficient is associated with SOC, thus the rate of its change is directly related to battery capacity. Therefore, taking into account typical capacity values (for instance 100 a/h at 48v) it can be concluded that rate of change of Rd in practical system is very slow and virtually decoupled from the slowest dynamics in the control system. In other words, for the complete duration of the transient in the system, the change of Rd is negligible. In order to demonstrate the aforementioned statement analytically and also to study effects of changing range of adaptive droop on system stability, a small signal model is developed in following subsection.

D. Modeling and Small Signal Stability Analysis

For simplicity, a buck converter that supplies a dc load through a series LC filter is analyzed without losing any generalization. Here, an average method is used so that only the averaged dynamics have been considered and the high frequency switching dynamics are neglected. The simplified buck converter is modeled as shown in Fig. 8(a). The dc load can be a combination of resistive electronic loads and negative impedance of CPLs. Mathematical model of the averaged buck converter can be described as follows [22]:

$$\begin{cases} L\frac{di_L}{dt} = (duty \cdot v_{in}) - v_{dc} - i_L \cdot R_s \\ C\frac{dv_{dc}}{dt} = i_L - \frac{v_{dc}}{R_L} \end{cases} \tag{4}$$

with R_L being the total equivalent resistance seen by the system. C, L and R_s are the converter output capacitance, inductance and inductor losses, respectively. Then, the corresponding transfer function is given as

$$\frac{v_{dc}(s)}{duty \cdot v_{in}(s)} = \frac{1}{LC \cdot s^2 + (R_s C + \frac{L}{R_L}) \cdot s + (1 + \frac{R_s}{R_L})} \tag{5}$$

The location of the LC filter poles should be investigated in order to study the stability of the buck converter. The mathematical model of (4) is represented as a block diagram in Fig. 8(b).

Using the derived model, a simplified current control loop is developed and the block diagram is presented in Fig. 9. A reduced order diagram can be constructed using the reasonable simplification in which PI current regulator is tuned to cancel the dominant pole introduced by $R_s - L$ load [21]. Therefore, the simplified current control loop shown in Fig. 9 can be represented as a first-order transfer function with time constant of three times higher than the system sampling time. Similarly, the voltage control loop can be modeled with the block diagram of Fig. 10. The block diagram shows that the current control loop is modeled using the first order transfer function.

As mentioned before, RESs can be controlled with MPPT algorithms (CPSs), while batteries can use charging control

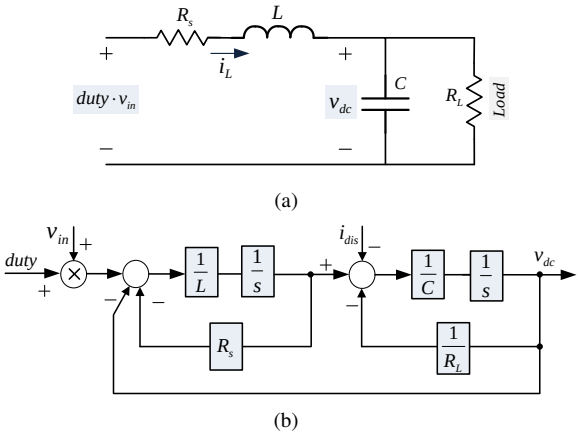

Fig. 8. Representing the averaged dynamics of a buck converter. (a) Equivalent circuit, (b) Block diagram

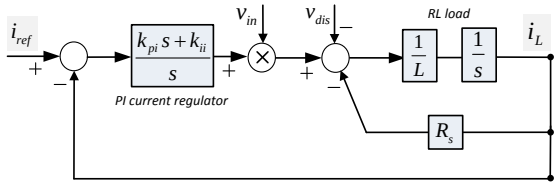

Fig. 9. Block diagram of the current control loop.

strategies (CPLs), however, both can be regulated by droop as well. An ideal CPS is modeled as a positive incremental impedance and negative current source, while a perfect CPL can be represented as a negative impedance in parallel with positive current source. A complete expression for current of a perfect CPL is as follows [22]:

$$i = \frac{1}{R_{CPL}} \cdot v + I_{CPL} \tag{6}$$

where $R_{CPL} = -\frac{V^2}{P_{CPL}}$ and $I_{CPL} = 2 \cdot \frac{P}{V}$ for a given operating point of $I = \frac{P}{V}$.

The negative impedance of CPLs decreases damping of the system, while the positive resistance of CPSs enhances the stability. Moreover, the constant current sources have no effect on the stability [22]. Taking the mentioned considerations into account, we can conclude that by modeling droop control loop and considering CPLs in the model, small signal stability analysis of the primary control is covered without losing generalization. Thus, if stability can be ensured in this worse case, MG should be stable in all other cases.

Fig. 11 presents block diagram of primary control for an individual dc-dc converter inside a MG. In this diagram, R_L represents equivalent load that can be combination of a resistive electronic load with positive or negative impedances produced by CPSs or CPLs, and Rd depicts the adaptive droop coefficient. By extracting the state space model of the

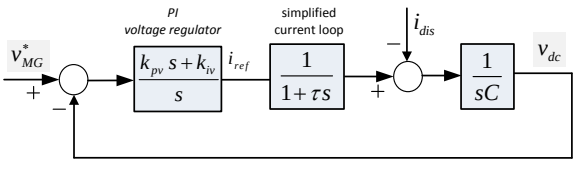

Fig. 10. Block diagram of voltage control loop.

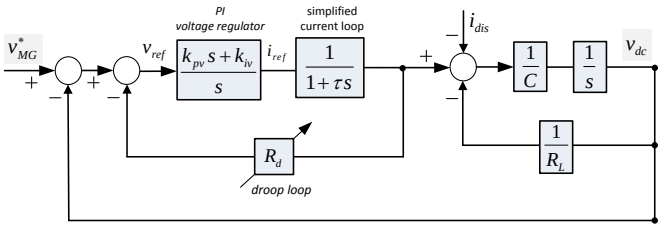

Fig. 11. Block diagram of primary control.

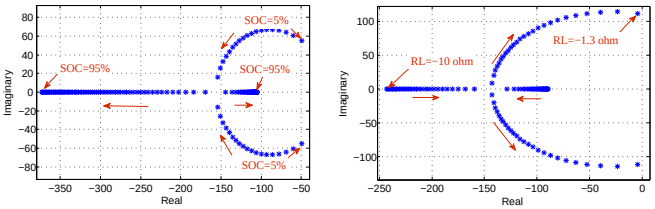

(a) (b)

Fig. 12. Family of the closed-loop critical eigenvalues of the system for: (a) SOC change, (b) Changing negative impedance of a CPL.

system from the presented block diagram, impact of negative resistance of CPLs, adaptive droop, and other parameters of control loops on the system stability can be easily investigated [29].

A system with sampling time $T_s = 0.1\ ms$, $L = 1.8\ mH$, $R_s = 2\ m\Omega$, and $C = 2.2\ mF$ was simulated and tested using the developed model. Fig. 12(a) shows movement of the critical poles of the system when droop coefficient is changed due to variation of SOC from 5% to 95% with respect to (2). It can be seen that the pole clusters move towards the left half of the s-plane enhancing the stability of system when SOC is increased. Opposite effect can be observed for discharging mode as increasing SOC in this mode will result in reducing droop coefficient (see Fig. 3). To that end, increasing R_d will improve stability of system since droop control acts as an active damping loop. Fig. 12(b) indicates the root locus graph of the system under gradual change of the negative impedance of a CPL from $-10\ \Omega$ to $-1.3\ \Omega$. As can be observed, the close loop dominant eigenvalues travel toward the right hand side of the s plane as negative impedance of CPL increases, which indicates unstable condition for the system. In order to validate the root locus graph shown in Fig. 12(b), simulation result is presented in Fig. 13. This figure shows bus voltage of a MG for different load change scenarios while droop control regulates the voltage around the reference which is 48 V.

It should be noted that as DC MGs are connected to the grid through an inverter which normally acts as a CSC, similar stability analysis could be used for grid connection mode.

IV. Distributed Control of Voltage and Power Flow in Dc Microgrid Clusters

In dc MGs, a more realistic scenario to achieve a higher quality of service and to enhance reliability is interconnection of several sources inside the MG or MGs together through the use of low-bandwidth communication on upper control layers. Using the communication interface, MG will be able to employ higher control levels such as secondary, tertiary or

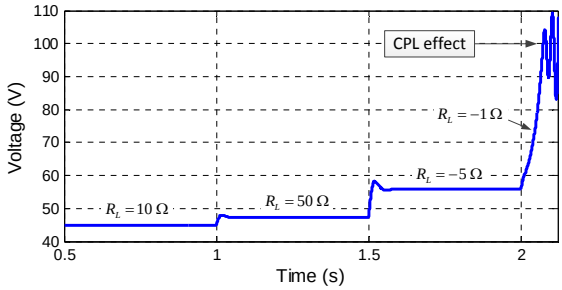

Fig. 13. Impact of negative impedance of CPLs on stability of a MG.

supervisory control on the top of primary one, thus obtaining full control over voltage, current, and power flow.

Due to disbalance between power consumption and production, droop control introduces deviation of the common dc bus voltage. Therefore, a secondary voltage controller is required to restore the voltage of the system to the acceptable range. This controller removes the voltage deviations inside the MG by sending an appropriate set-point to the droop control units. This signal changes the voltage reference of droop unit(s) accordingly by shifting the droop line up and down. On the other hand, in the case of connecting the MG to the other MGs or dc bus, another controller must be employed to control the power/current flow. It is obvious that power flow control can be accomplished only when MG bus voltages are different.

In this paper, we propose a consensus-based distributed control framework that regulates the voltages across the MGs within an acceptable range while guaranteeing power flow control between them. Fig. 14 shows the proposed control methodology for a single MG, e.g., MG_i, which includes two separate modules; voltage regulator and power flow controller. The voltage regulator maintains the average voltage of the whole cluster at the rated value, while the power flow controller monitors the SOC of batteries in the MGs and adjusts power flow references accordingly. The proposed voltage regulator aims to regulate the average voltage of the whole cluster, rather than individual MG buses. Moreover, when a MG operates individually without connecting to its neighbors, the voltage regulator acts as a central controller, termed as centralized voltage secondary control (CVSC), to provide smooth connection of MGs by removing voltage deviation of buses.

Different distributed policies are proposed for two introduced modules as discussed in the following subsections. In the proposed methodology, the controllers are linked through a communication network. This communication network which is spanned across the cluster, enables data exchange among the controllers. Each controller e.g. controller at Node i, relays an information vector to its neighbors on the network. The information vector includes estimated average of voltage across the cluster (v_i^{avg}), and SOC of batteries inside MGs (SOC_i). Each controller receives data from its neighbors on graph and, after local processing of the information, it updates its control variables.

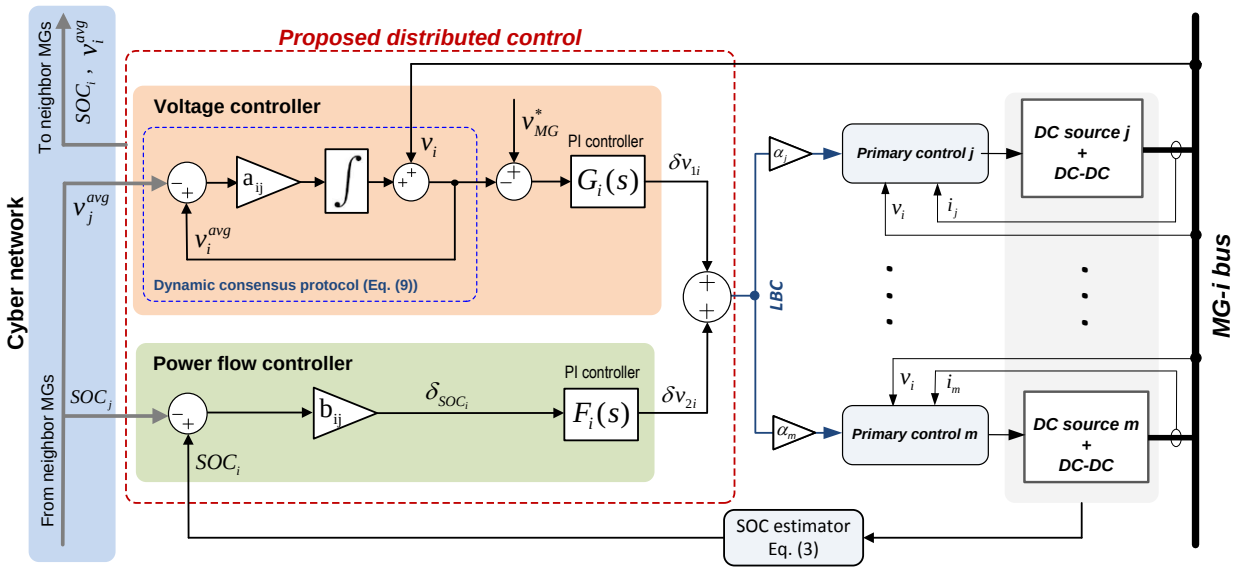

Fig. 14. Proposed hierarchical control for multiple DC microgrid clusters.

A. Consensus in Graphs

We consider a network of communication links consisting of a set of nodes $V = \{v_1, v_2, ..., v_N\}$ connected through a set of edges $E = V \times V$, where N is number of nodes. Such a network can be represented by a graph $G = (V, E)$, as shown in Fig. 15. Each node is assigned with a MG in the cluster, and edges represent communication links for data exchange. Each node can only communicate with its direct neighbors. The communication graph does not require having the same topology as the underlying physical MGs. A matrix called adjacency matrix $A = [a_{ij}]$ is associated to the edges. a_{ij} represents the weight for information exchanged between agents i and j, where $a_{ij} > 0$ if agents i and j are connected through an edge $(v_j, v_i) \in E$, otherwise, $a_{ij} = 0$. The set of neighbors of node i is denoted N_i. Equivalently, if $j \in N_i$, then v_i receives information from v_j. However, the links are not necessarily bidirectional. If communication links are bidirectional, $(v_i, v_j) \in E \Rightarrow (v_j, v_i) \in E, \forall i, j$ the graph is said to be undirected, otherwise it is directed, and also termed a digraph. The laplacian matrix is defined as $L = D^{in} - A$, and its eigenvalues determine the global dynamics of the system. $D^{\text{in}} = \text{diag}\{d_i^{\text{in}}\}$, called in-degree matrix, is a diagonal matrix where $d_i^{\text{in}} = \sum_{j \in N_i} a_{ij}$. A graph is called balanced if the total weight of edges entering a node and leaving the same node are equal for all nodes [15]. A digraph is said to have a spanning tree if it contains a root node, from which there exists at least one direct path to every other node.

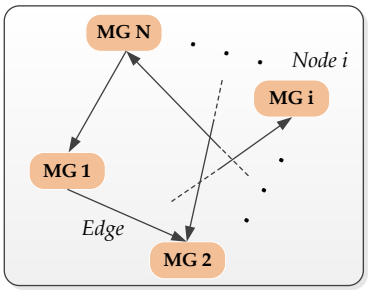

Fig. 15. Communication network spanned across Microgrids for data exchange.

According to [15], a simple consensus algorithm to reach an agreement regarding continuous time integrator agents with dynamics $\dot{x}_i = u_i$ can be expressed as a distributed linear consensus protocol on a graph

$$\dot{x}_i(t) = \sum_{j \in N_i} a_{ij}(x_j(t) - x_i(t)) \tag{7}$$

The consensus value for protocol (7) can be, for instance, the average of the initial values, $(1/n)\sum_{i=1}^{n} x_i(0)$. Then, the collective dynamics of the group of agents can be written as

$$\dot{x} = -Lx \tag{8}$$

The convergence speed is determined based on laplacian matrix (L) [15]. Thus, the weights need to be well designed in order to obtain faster convergence. For networks like power systems and Microgrids, L can be designed to be symmetrical, i.e., $a_{ij} = a_{ji}$, in order to have plug-and-play and link failure resiliency features.

B. Voltage Control

Inspired by [13], a distributed voltage secondary control (DVSC) strategy is proposed here based on dynamic consensus protocol [30], in order to regulate the voltage in the MGs buses. As highlighted in Fig. 14, this voltage regulator provides a voltage correction term, δv_{1i}, to be added to droop control units of MG_i, in order to restore the voltage at node i. Each controller uses dynamic consensus protocol to estimate the average of voltages across the cluster. The distributed protocol at each node (here Node i) is expressed as

$$\dot{v}_i^{avg}(t) = \sum_{j \in N_i} a_{ij}(v_j^{avg}(t) - v_i^{avg}(t)) + \dot{v}_i(t) \tag{9}$$

where v_i is the measured voltage at Node i, v_i^{avg} is the estimation of the averaged voltage provided by the estimator

at Node i, and v_j^{avg} is the estimation of voltage received from neighbor Node j. The estimated voltage is then compared with the reference voltage, v_{MG}^*, which is normally the rated voltage of the MG, and fed to a PI controller, $G_i(s)$, to generate the voltage correction term, δv_{1i} (see Fig. 14).

Implementation of the presented protocol in (9) is shown in Fig. 14. As seen in this figure, the local voltage, v_i, is used in the estimation process. This way, any voltage variation at any node, e.g., Node i, would immediately affect the estimation at that node, v_i^{avg}. It is shown in [30] that if the communication graph is balanced and contains at least a spanning tree, all estimations converge to a global consensus, which is the average value. Therefore, by choosing appropriate communication graph, all estimations will converge to the true average of voltages across the cluster.

Dynamic consensus protocol presented in [13] has been used to estimate the global average voltage in order to regulate bus voltages inside a dc MG. However, the one presented here is utilized to regulate the voltage across the whole dc MG clusters. In addition, the voltage regulator proposed here can operate in two ways; centralized for the units inside each MG where it is able to remove voltage deviations inside each individual MG, and distributed over the neighbor MGs when they are connected together to maintain MGs voltages around the reference. This way, the average voltage of all MG buses equals to the reference with an option to control current flow between the connected MGs since voltage levels could be different.

C. Power Flow Control

Expansion of a MG in terms of increase of load can be achieved by an expansion of energy sources and storage capacity. However, connection to the other neighbor MGs could be a better possibility as it is not practical to add new production or storage to existing arrangement. A MG can be made more reliable by interconnecting to the neighbor MGs, creating MG clusters.

Once MGs are connected to each other (or to a stiff dc source), current/power flow between them requires to be managed. Power flow can be controlled by changing the level of voltage inside the MGs. To accomplish this goal, we propose a distributed power flow control (DPFC) over MGs so that each MG controls the tie-line with its neighbors according to a reference. As load profile or production of a MG might be changed, it is therefore not viable to use a predefined reference for current flow between MGs. It is felt by the authors that a good solution is to deploy SOC of batteries to define the reference, as it states the cumulative difference between production and consumption of the system. It should be mentioned that SOC of batteries inside each MG is equalized using the proposed adaptive droop control as presented in Section III, hence SOC of any battery represents SOC level of the MG. In order to apply this idea, in a cluster of MGs where each MG consists of arbitrary number of batteries, a MG with the highest average SOC should participate more in the current flow, injecting the highest current to its neighbors, while a MG with the lowest one absorbs the maximum current from the others.

The power flow controller at Node i, receives SOC of all its neighbors, e.g. the terms SOC_j from all Nodes j, $j \in N_i$. Then it compares its SOC, SOC_i, with the neighbors SOC to calculate the SOC mismatch, δ_{SOC_i}, as follows

$$\delta_{SOC_i} = \sum_{j \in N_i} b_{ij}(SOC_i - SOC_j) \tag{10}$$

where b_{ij} is adjacency matrix, which determines the power flow control dynamics. Needless to mention that it is also possible to use a coupling gain between two proposed distributed controllers to be able to use the same communication infrastructure. The SOC mismatch, δ_{SOC_i}, is passed through an standard PI controller, $F_i(s)$, to generate the second voltage correction term, δv_{2i}. This PI controller helps the consensus protocol in (10) to lower the SOC mismatch among neighbors' MGs and, ultimately, make them all converge to the same value. Equivalently, the SOCs converge to a global consensus, and current/power will be regulated between the MGs accordingly.

It should be noted that the voltage correction terms, δv_{1i} and δv_{2i}, must be limited, as large values might affect system stability. These correction terms can be also distributed along the sources inside each MG, passing through a participation factor (α). Participation factor of batteries, for instance, can be according to their SOC and for RESs based on their power rate ($0 < \alpha \leq 1$).

D. Dynamic Model

To study small signal stability analysis and to investigate impact of different parameters of the system on the stability, the developed model for dc MGs is expanded for multiple dc MG clusters. The model has been developed for two interconnected MGs including all control loops, as depicted in Fig. 16. For simplicity, only one droop controlled unit is considered inside each MG since it can represent a whole group of droop regulated units as already discussed. The distributed secondary control loops are then added to the primary loop. In the developed model, $G_i(s)$ and $F_i(s)$ are typical PI controllers used for voltage and power flow regulation. As can be seen in Fig. 16, estimation of SOC is included in the model in order to analyze the distributed power flow control. As the figure shows, multiplication of inductor current with duty ratio is required for SOC estimation, because SOC change is associated with primary side current of buck converter. However, as power flow regulation is based on differences of SOCs in the MGs and SOC changes is really slow, fast dynamic of duty ratio is virtually completely absorbed by the slow SOC integrator. Therefore, duty ratio was considered constant here with value 0.48. Using the presented block diagram, a state space model with 15 state variables is extracted accordingly to evaluate impact of different parameters on the system stability. Due to page limitation details of developed state space model is not presented in the paper.

As already mentioned, SOC dynamic is completely decoupled from the slowest dynamic in the control system which is voltage regulation loop here. This can be now confirmed with the root locus in Fig. 17, in which the red poles are associated

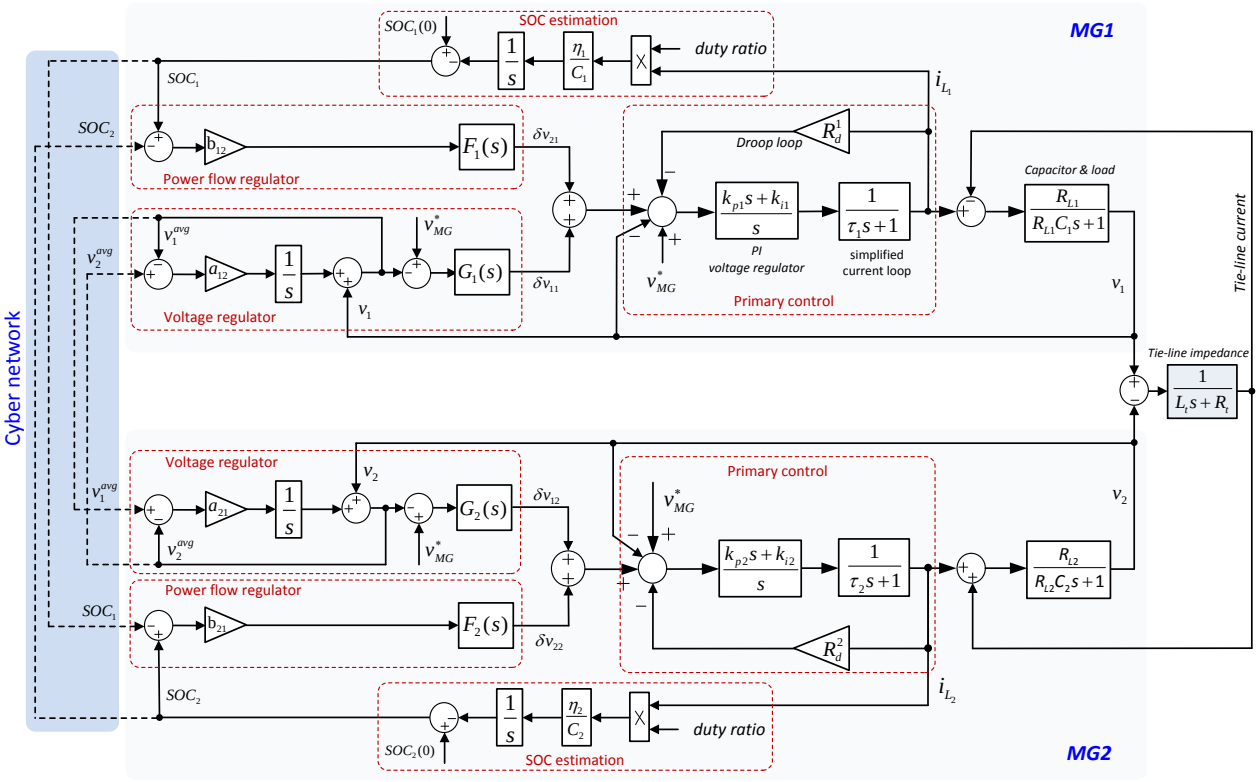

Fig. 16. Small signal model of two interconnected MGs with all control loops.

with SOCs. It can be seen that those poles are far away from the remaining poles of the system.

When connecting MGs, stability of system might be influenced by the impedance of interconnected line. To study this effect, tie-line impedance has been also taken into account in the model. Here, L_t and R_t are the inductance and resistance of interconnected line between MGs, respectively. As the block diagram shows, tie-line current is added to the input of RC filter as a disturbance. Fig. 18 shows the behavior of system eigenvalues when inductance of interconnected line changes between $0.5\ mH$ and $4\ mH$. It is shown that if the line inductance becomes bigger, the system moves toward unstable region. Similar behavior can be observed when line resistance gets smaller. Therefore, it is obvious that stability of system is influenced depending on the impedance of tie-lines. Using this model, impact of other parameters of system on the stability can be easily examined.

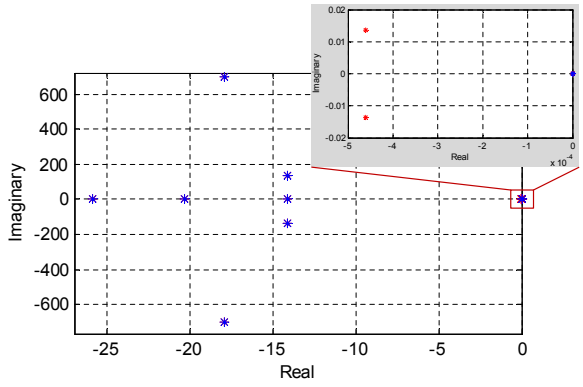

Fig. 17. Family of the closed-loop eigenvalues of the interconnected MGs with (red) and without (blue) SOC dynamics.

V. Results

Hardware-in-the-loop (HIL) simulation results of three interconnected dc MGs are presented here in order to show the feasibility of the proposed hierarchical control. As shown in Fig. 19, MGs are connected through resistive-inductive lines, and each MG consists of four units which are supporting some loads. PV and WT work in MPPT and two batteries work in droop controlled mode. For the simulation setup, the MGs nominal voltage was selected at 48 V. A communication network, as shown in Fig. 19, facilitates cooperation of the MGs. Each MG can only communicate with its immediate

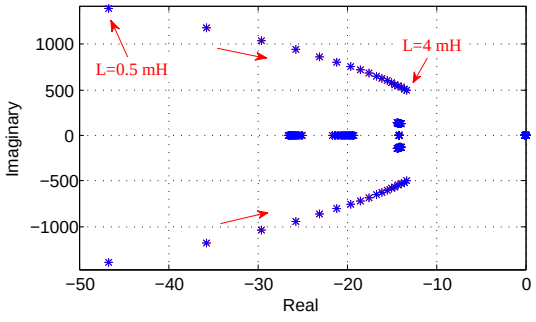

Fig. 18. Family of the closed-loop eigenvalues of the interconnected MGs for different value of line inductance.

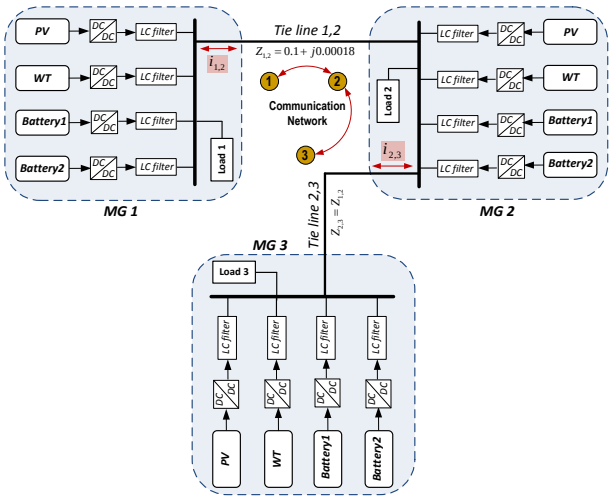

Fig. 19. HIL simulation case study: Three interconnected DC Microgrids.

TABLE I
ELECTRICAL SETUP AND CONTROL SYSTEM PARAMETERS

Parameter	Symbol	Value
Electrical parameters		
dc power supply	Vin	100 V
Input capacitance	C	2.2e-3 F
Converter inductances	L	1.8e-3 H
Inductor+switch loss resistance	R_s	0.2 Ω
Tie-line inductance	L_t	1.8e-3 mH
Tie-line resistance	R_t	0.1 Ω
Switching frequency	f_s	10 kHz
Primary Control		
Reference voltage	v^*_{MG}	48 V
Proportional current term	k_{pi}	5
Integral current term	k_{ii}	560
Proportional voltage term	k_p	1.2
Integral voltage term	k_i	97
Fixed droop coefficient	R_d	0.5
Voltage and Power flow control		
proportional voltage term	k_{ps}	0.1
Integral voltage term	k_{is}	20
proportional power flow term	k_{pt}	0.5
Integral power flow term	k_{it}	10

neighbor, e.g. the one which is connected to it through electrical lines. The links are assumed bidirectional to feature a balanced Laplacian matrix. The proposed distributed hierarchical control loops were developed in Matlab/Simulink. However, the final code was compiled into a dSPACE ds1006 platform in order to have HIL simulations. Associated adjacency matrices of communication network, for voltage regulator, $\mathbf{A}$, and power flow controller, $\mathbf{B}$, are

$$\mathbf{A} = \begin{bmatrix} 0 & 20 & 0 \\ 20 & 0 & 20 \\ 0 & 20 & 0 \end{bmatrix}, \mathbf{B} = \begin{bmatrix} 0 & 2 & 0 \\ 2 & 0 & 2 \\ 0 & 2 & 0 \end{bmatrix}. \quad (11)$$

Other electrical and control parameters are listed in Table I.

Fig. 20 shows a set of waveforms derived from implementation of proposed hierarchical scheme. In this figure, the voltage regulator is added to the all MGs in the first 2 s, and after connecting MGs, power flow control is activated in the second half of operation. In the first scenario of simulation, only

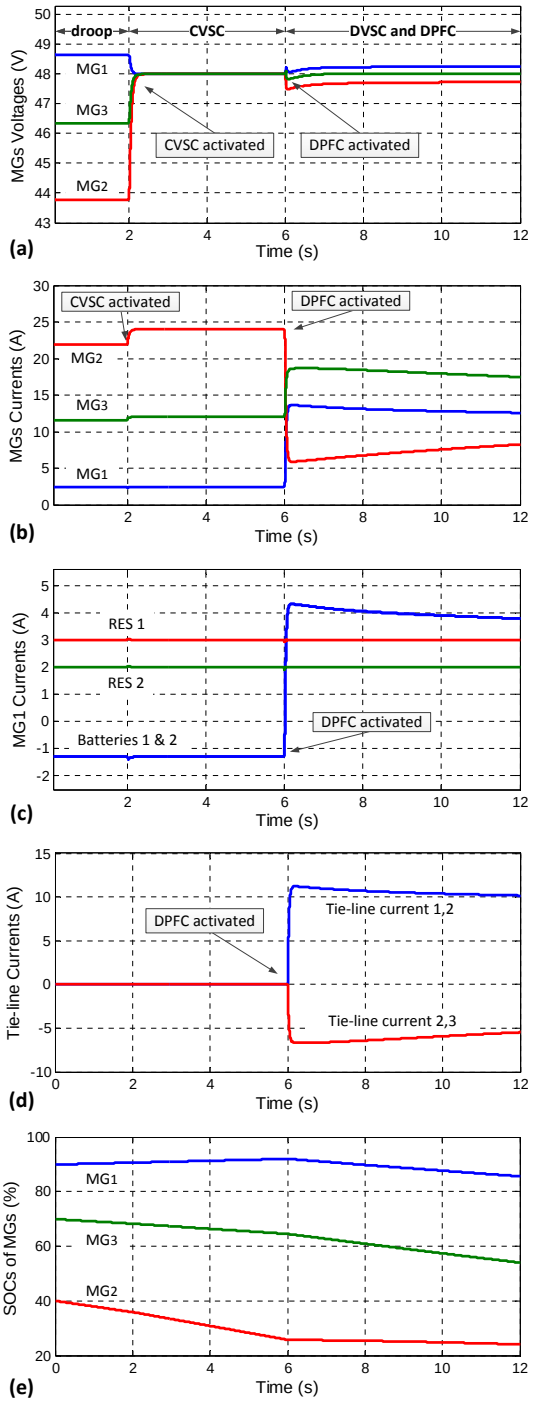

Fig. 20. Performance of the proposed voltage and power flow controllers.

primary control operates inside the system and the MGs are disconnected having no current flow. In this period, different voltage deviations can be observed due to mismatch between production and consumption created by the droop control, since MGs are supporting different amount of loads, $20-$, $2-$, and $4-\Omega$ respectively; MG_2 injects about 22 A current which is approximately double of injected current by MG_3, while MG_1 feeds small amount of current, (see Fig. 20(b)). Fig. 20(c) indicates currents of MG_1 sources. As can be seen, RESs inject constant amount of current to support the local load while the extra power is used to charge the batteries. At

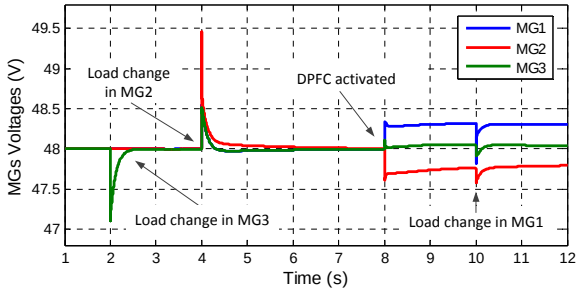

Fig. 21. Performance of the proposed strategies in rejecting load disturbances.

$t = 2s$, the voltage regulator which is centralized for MGs individually, starts to act to remove the voltage deviations. As can be seen, it is able to eliminate steady state errors of bus voltages properly when MGs are not connected. Fig. 20(b) shows that MGs currents increase slightly, depending on the amount of deviation in each MG, in order to support the voltage controller action.

In the second scenario, MGs are connected at $t = 3s$ and $t = 4s$, however, no current flows between them as there is no voltage difference in the MGs. As a result, one can conclude that connection of MGs could be quite smooth having no effect on the system stability, if we activate the voltage controller before connection. After activating the DPFC in the middle of simulation, current references produced by the proposed distributed policy in (10) are imposed by this controller to be injected from MG_1 and MG_3 respectively (see Fig. 20(d)), by producing some voltage deviation in the MGs buses. At this moment, MGs currents change accordingly, as shown in Figs. 20(b) and 19(c), following the DPFC action. As can be observed, as soon as DPFC is added at $t = 6s$, the voltage regulators become distributed over the MGs in order to have current flow between the MGs. This way, the MGs bus voltages remain within an acceptable range while DPFC regulates the current flow according to SOC of batteries inside the MGs.

Fig. 20(e) represents total averaged SOCs of batteries in the MGs for different scenarios. The rate of charge/discharge changes when DPFC starts to act, as power/current reference is determined according to the SOCs; for instance MG_1 starts to be discharged with high rate while discharging rate of MG_2 decreases significantly. Moreover, the amount of tie-line currents get smaller as total SOCs of MGs trend to be equalized based on the proposed policy. It is worth mentioning that SOC of batteries inside each MG are equalized using the adaptive droop method as explained in Section III.

Fig. 21 indicates the performance of proposed control strategies in rejecting load disturbances (50% changes) inside the MGs before and after connection. MGs are connected at $t = 3s$ and $t = 3.5s$ respectively, and DVSC starts acting at $t = 8s$ as a result of activating the DPFC. For simplicity, only voltage waveforms are presented in Fig. 21. As can be observed, the distributed voltage regulator is able to eliminate the load disturbances properly.

As the proposed distributed strategies use neighboring communication, delay will have a significant impact on their performance. Efficacy of the controllers is examined here for

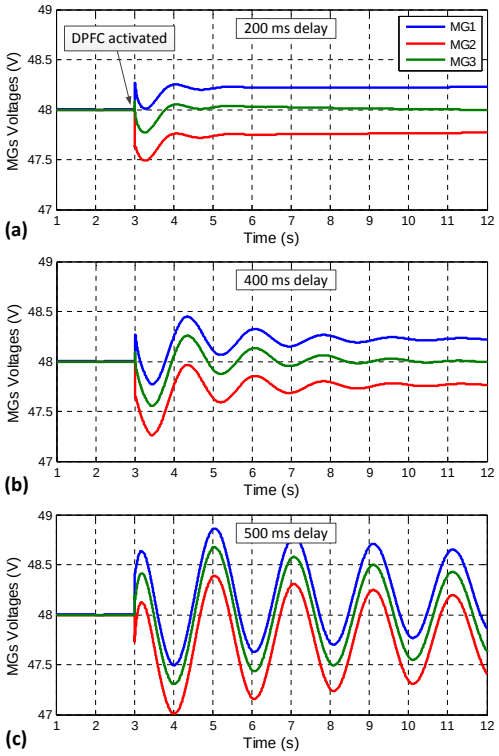

Fig. 22. Impact of communication delay on the performance of proposed controllers.

different amount of fixed communication latency, 200 ms, 400 ms and 500 ms. Fig. 22 shows the effect of mentioned communication delays on the voltage controller response when it tries to maintain the voltage around the reference. The voltage regulator operates independent for each MG at the beginning, and then becomes distributed among the MGs when DPFC is added at $t = 3s$. As can be seen, the control system response starts to have oscillations by considering bigger communication delays and take the system toward instability when there exists communication delay of 500 ms.

VI. Conclusion and Discussion

In this paper, a hierarchical control scheme is introduced for dc MG clusters. In the primary level, a SOC based adaptive droop function is proposed to define droop coefficient automatically, resulting in SOC equalization. A small signal model is developed to study impact of system parameters on the stability. The upper level of control on each MG has two modules; the voltage regulator and the power flow controller. The voltage regulator is implemented in a centralized way inside each MG to ensure smooth connection of MGs, as it eliminates the entire deviations in the MG bus voltages. However, power flow control is impossible to achieve due to the fact that power flow between the MGs is obtained at the expense of voltage deviations. To cope with this, dynamic consensus method is utilized for the voltage regulator to make it distributed over the MGs when power flow control is required. The power flow controller compares local SOC with its MG neighbors SOCs using a cooperative policy and, accordingly, adjusts the voltage set point for droop in order to

carry out appropriate power flow. This way, MGs tend to have equal SOCs despite of having different amount of loads. This control methodology uses a sparse communication network for data exchange. In order to analyze the system stability and also to tune the proposed control control parameters, the small signal model was expanded for interconnected dc MGs including all the control loops. Simulation studies show that the proposed control paradigm successfully carries out the global voltage regulation and power flow control in dc MG clusters and guarantees stable operation of these systems.

REFERENCES

[1] H. Kakigano, Y. Miura, and T. Ise, "Low-voltage bipolar-type dc microgrid for super high quality distribution," *IEEE Trans. Power Electron.*, vol. 25, no. 12, pp. 3066–3075, Dec 2010.

[2] A. Kwasinski, "Quantitative evaluation of dc microgrids availability: Effects of system architecture and converter topology design choices," *IEEE Trans. Power Electron.*, vol. 26, no. 3, pp. 835–851, March 2011.

[3] T. Dragicevic, J. M. Guerrero, and J. C. Vasquez, "A distributed control strategy for coordination of an autonomous LVDC microgrid based on power-line signaling," *IEEE Trans. Ind. Electron.*, vol. 61, no. 7, pp. 3313–3326, July 2014.

[4] R. S. Balog and P. T. Krein, "Bus selection in multibus dc microgrids," *IEEE Trans. Power Electron.*, vol. 26, no. 3, pp. 860–867, March 2011.

[5] K. Sun, L. Zhang, Y. Xing, and J. M. Guerrero, "A distributed control strategy based on dc bus signaling for modular photovoltaic generation systems with battery energy storage," *IEEE Trans. Power Electron.*, vol. 26, no. 10, pp. 3032–3045, Oct 2011.

[6] D. Salomonsson, L. Soder, and A. Sannino, "Protection of low-voltage dc microgrids," *IEEE Trans. Power Del.*, vol. 24, no. 3, pp. 1045–1053, July 2009.

[7] J. M. Guerrero, M. Chandorkar, T. Lee, and P. C. Loh, "Advanced control architectures for intelligent microgrids—part I: Decentralized and hierarchical control," *IEEE Trans. Ind. Electron.*, vol. 60, no. 4, pp. 1254–1262, April 2013.

[8] N. R. Chaudhuri and B. Chaudhuri, "Adaptive droop control for effective power sharing in multi-terminal dc (MTDC) grids," *IEEE Trans. Power Syst.*, vol. 28, no. 1, pp. 21–29, Feb 2013.

[9] N. Diaz, T. Dragicevic, J. C. Vasquez, and J. M. Guerrero, "Intelligent distributed generation and storage units for dc microgrids–a new concept on cooperative control without communications beyond droop control," *IEEE Trans. Smart Grid*, vol. 5, no. 5, pp. 2476–2485, Sept 2014.

[10] X. Lu, K. Sun, J. M. Guerrero, J. C. Vasquez, and L. Huang, "State-of-charge balance using adaptive droop control for distributed energy storage systems in dc microgrid applications," *IEEE Trans. Ind. Electron.*, vol. 61, no. 6, pp. 2804–2815, June 2014.

[11] T. Dragicevic, J. M. Guerrero, J. C. Vasquez, and D. Skrlec, "Supervisory control of an adaptive-droop regulated dc microgrid with battery management capability," *IEEE Trans. Power Electron.*, vol. 29, no. 2, pp. 695–706, Feb 2014.

[12] X. Lu, K. Sun, J. M. Guerrero, J. C. Vasquez, and L. Huang, "Double-quadrant state-of-charge-based droop control method for distributed energy storage systems in autonomous dc microgrids," *IEEE Trans. Smart Grid*, Early Access.

[13] V. Nasirian, S. Moayedi, A. Davoudi, and F. L. Lewis, "Distributed cooperative control of dc microgrids," *IEEE Trans. Power Electron.*, Early Access.

[14] Q. Shafiee, C. Stefanovic, T. Dragicevic, P. Popovski, J. C. Vasquez, and J. M. Guerrero, "Robust networked control scheme for distributed secondary control of islanded microgrids," *IEEE Trans. Ind. Electron.*, vol. 61, no. 10, pp. 5363–5374, Oct 2014.

[15] R. Olfati-Saber, J. A. Fax, and R. M. Murray, "Consensus and cooperation in networked multi-agent systems," *Proceedings of the IEEE*, vol. 95, no. 1, pp. 215–233, Jan 2007.

[16] T. C. Aysal, M. E. Yildiz, A. D. Sarwate, and A. Scaglione, "Broadcast gossip algorithms for consensus," *IEEE Trans. Signal Process.*, vol. 57, no. 7, pp. 2748–2761, July 2009.

[17] S. Anand, B. G. Fernandes, and M. Guerrero, "Distributed control to ensure proportional load sharing and improve voltage regulation in low-voltage dc microgrids," *IEEE Trans. Power Electron.*, vol. 28, no. 4, pp. 1900–1913, April 2013.

[18] X. Lu, J. M. Guerrero, K. Sun, and J. C. Vasquez, "An improved droop control method for dc microgrids based on low bandwidth communication with dc bus voltage restoration and enhanced current sharing accuracy," *IEEE Trans. Power Electron.*, vol. 29, no. 4, pp. 1800–1812, April 2014.

[19] S. Moayedi, V. Nasirian, F. Lewis, and A. Davoudi, "Team-oriented load sharing in parallel dc-dc converters," *IEEE Trans. Ind. App.*, Early Access.

[20] L. Meng, T. Dragicevic, J. M. Guerrero, and J. C. Vasquez, "Dynamic consensus algorithm based distributed global efficiency optimization of a droop controlled dc microgrid," in *IEEE Energy Conference (ENERGYCON14)*, May 2014, pp. 1276–1283.

[21] V. Blasko and V. Kaura, "A new mathematical model and control of a three-phase ac-dc voltage source converter," *IEEE Trans. Power Electron.*, vol. 12, no. 1, pp. 116–123, Jan 1997.

[22] A. M. Rahimi and A. Emadi, "Active damping in dc/dc power electronic converters: A novel method to overcome the problems of constant power loads," *IEEE Trans. Ind. Electron.*, vol. 56, no. 5, pp. 1428–1439, May 2009.

[23] A. Kwasinski and C. N. Onwuchekwa, "Dynamic behavior and stabilization of dc microgrids with instantaneous constant-power loads," *IEEE Trans. Power Electron.*, vol. 26, no. 3, pp. 822–834, March 2011.

[24] D. Boroyevich, I. Cvetkovic, D. Dong, R. Burgos, F. Wang, and F. Lee, "Future electronic power distribution systems a contemplative view," in *Proc. 12th Opt. Electric. and Electron. Equip. (OPTIM)*, May 2010, pp. 1369–1380.

[25] T. Esram and P. L. Chapman, "Comparison of photovoltaic array maximum power point tracking techniques," *IEEE Trans. Energy Convers.*, vol. 22, no. 2, pp. 439–449, June 2007.

[26] T. David Linden, *Handbook of Batteries*, McGraw Hill, 2002.

[27] M. Coleman, C. K. Lee, C. Zhu, and W. G. Hurley, "State-of-charge determination from emf voltage estimation: Using impedance, terminal voltage, and current for lead-acid and lithium-ion batteries," *IEEE Trans. Ind. Electron.*, vol. 54, no. 5, pp. 2550–2557, Oct 2007.

[28] T. Dragicevic, H. Pandzic, D. Skrlec, I. Kuzle, J. M. Guerrero, and D. S. Kirschen, "Capacity optimization of renewable energy sources and battery storage in an autonomous telecommunication facility," *IEEE Trans. Sustain. Energy*, vol. 5, no. 4, pp. 1367–1378, Oct 2014.

[29] Q. Shafiee, T. Dragicevic, J. C. Vasquez, and J. M. Guerrero, "Modeling, stability analysis and active stabilization of multiple dc-microgrid clusters," in *IEEE Intern. Energy Conf. (ENERGYCON 14)*, May 2014, pp. 1284–1290.

[30] D. P. Spanos, R. Olfati-Saber, and R. M. Murray, "Dynamic consensus for mobile networks," in *Proc. 16th Int. Fed. Aut. Control (IFAC)*, 2005, pp. 1–6.